

# Efficient detection of single molecules eluting off an optically trapped microsphere

Nicholas P Machara<sup>†</sup>, Peter M Goodwin<sup>‡</sup>, Jörg Enderlein<sup>§</sup>,  
David J Semin<sup>||</sup> and Richard A Keller

Chemical Science and Technology Division, Mail Stop M888,  
Los Alamos National Laboratory, Los Alamos NM 87545, USA

Submitted 24 November 1997, accepted 15 December 1997

**Abstract.** We demonstrate efficient detection of single fluorescent molecules eluting off a polystyrene microsphere optically trapped in a flowing sheath stream. A 1  $\mu\text{m}$  diameter analyte doped microsphere was positioned  $\sim 20 \mu\text{m}$  upstream of a 16  $\mu\text{m}$  diameter probe laser without significant degradation of the detection signal-to-noise ratio due to scattered laser light and fluorescence from the microsphere. In comparison to more standard capillary sample introduction, the microsphere causes only small perturbations to the sheath fluid flow. The small diameter of the analyte stream eluting from the microsphere results in a greater than 90% detection efficiency for single rhodamine-6G molecules, limited primarily by the photostability of the dye.

**Keywords:** single molecule detection, laser-induced fluorescence, optical trap

## 1. Introduction

We have demonstrated single molecule detection (SMD) by recording fluorescence bursts from individual molecules as they flow through a focused laser beam [1]. Subsequently, several other groups have demonstrated this capability with flowing and static samples. Several articles reviewing the progress in this field have been published recently [2–4].

As a fluorescent molecule crosses an excitation laser beam it emits a burst of photons. Fluorescence bursts from single molecules are detected in the presence of background due to Raman and Rayleigh scattered laser light as well as fluorescence from impurities dissolved in the solvent. Most of the background due to scattered laser light can be removed by using pulsed excitation and time-gated detection [1, 5]. Small detection volumes (the illuminated solvent volume in the field of view of the detector) are used to improve the signal-to-background ratio

(SBR). Hydrodynamic focusing of the sample stream in a sheath flow cuvette [6], an excitation laser beam focused to  $\sim 10 \mu\text{m}$  ( $e^{-2}$  diameter), and a spatial filter in the detection path can be used to attain a detection volume of approximately 1 picoliter (pl). Under these conditions, molecules containing a single fluorochrome can be detected with excellent SBRs and high efficiencies limited mainly by the photostability of the fluorochrome [7, 8].

Working in the near-infrared (NIR) results in reduced backgrounds due to Raman scatter and impurity fluorescence [9]. Detection efficiencies greater than 95% have been reported for single NIR emitting dye molecules dissolved in methanol and confined in  $\sim 10 \mu\text{m}$  diameter capillaries [10, 11]. In these experiments the lateral dimensions of the detection volume were defined by the inner wall of the capillary.

Single molecule fluorescence SBRs can be improved further by using confocal excitation/detection techniques to attain diffraction-limited detection volumes of less than 1 femtoliter [12–15]. A major drawback to the use of such small volumes in applications requiring efficient detection of analyte is the difficulty of constraining all of the analyte molecules to flow through a volume with linear dimensions of  $\leq 1 \mu\text{m}$  [4]. To date, most investigations using such small volumes have relied on diffusion to transport analyte

<sup>†</sup> Present address: EM-30, US Department of Energy, 19901 Germantown Rd, Germantown, MD 20874-1290, USA.

<sup>‡</sup> To whom correspondence should be addressed.

<sup>§</sup> Present address: Institute of Analytical Chemistry, Chemo- and Biosensors, University of Regensburg, PO Box 101042, D-93040 Regensburg, Germany.

<sup>||</sup> Present address: Amgen Inc., 1840 DeHavilland Drive, Thousand Oaks, CA 91320, USA.

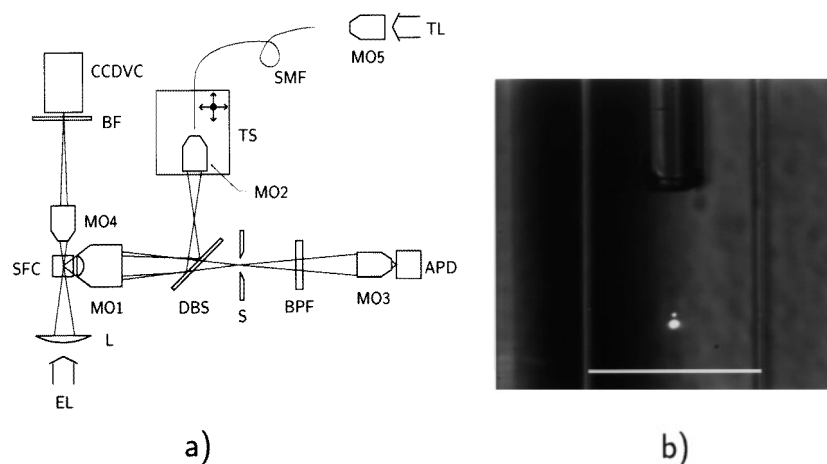


**Figure 1.** (a) The experimental apparatus schematic diagram. Legend: APD, single photon counting avalanche photodiode; BF, blocking filters; BPF, bandpass filter; CCDVC, charge coupled device video camera; DBS, dichroic beam splitter; EL, excitation laser; L, excitation laser focusing lens; MO1, optical trapping/fluorescence collection objective; MO2, trapping laser fiber output coupling objective; MO3, fluorescence imaging objective; MO4, imaging objective; MO5, trapping laser fiber input coupling objective; S, slit; SFC, sheath flow cuvette; SMF, single mode fiber; TL, trapping laser; TS, three-axis translation stage. (b) The sheath flow channel viewed along the excitation laser axis. The width of the square-bore flow channel is indicated by the white 250  $\mu\text{m}$  scale bar near the bottom of the picture. Sheath fluid flows from top to bottom. An optically trapped 1  $\mu\text{m}$  microsphere, illuminated with a HeNe laser (633 nm), is visible less than 20  $\mu\text{m}$  upstream of the focused (16  $\mu\text{m}$   $e^{-2}$  diameter) excitation laser beam. The end of the sample delivery capillary (90  $\mu\text{m}$  od, 20  $\mu\text{m}$  id) used for delivery of microspheres to the optical trap is visible  $\sim 200$   $\mu\text{m}$  upstream of the excitation laser.

molecules through the detection volume. A recent report demonstrated efficient detection of single rhodamine-6G (R6G) molecules dissolved in ethylene glycol flowing through a 1  $\mu\text{m}$  diameter microcapillary using confocal excitation/detection [16].

Efficient sample delivery to  $\sim 1$  pl volumes requires sample stream diameters less than 10  $\mu\text{m}$ . For sample flow velocities typically used for SMD ( $\sim 1$   $\text{cm s}^{-1}$ ), radial diffusion of analyte into the sheath fluid on the way to the detection volume can broaden the sample stream significantly [6, 17]. This is especially true for low molecular weight ( $< 1000$  amu) analytes. For rapidly diffusing analytes, one positions a tapered sample injection capillary ( $\sim 1$   $\mu\text{m}$  inner diameter (id)) as close to the detection volume as possible [7, 8]. Because of problems associated with scattered light and fluorescence from the capillary tip, it is difficult to position the capillary as close to the detection volume as one would like. There are other problems associated with capillary sample introduction. Perturbations of the sheath fluid flow by the capillary can broaden the sample stream (see later). Also, adsorbed fluorescent impurities released from capillary surfaces contribute to the background.

In this paper, we demonstrate efficient sample delivery to picoliter detection volumes from a 1  $\mu\text{m}$  diameter microsphere optically trapped  $\sim 20$   $\mu\text{m}$  upstream of the detection volume. Under these conditions, the analyte has only a short time to diffuse before reaching the probe volume resulting in reduced diffusional broadening of the sample stream. Peaked burst size distributions and SMD efficiencies greater than 90% were attained for R6G. We

calculate the evolution of sample stream diameters for a diffusing species eluting from the surface of a sphere and from the end of a prolate ellipsoid of revolution (a shape similar to the end of a pulled sample injection capillary [4]) under flow conditions similar to those of our experiments. These calculations demonstrate that the sample stream diameter from the sphere is significantly smaller than that from the ellipsoid due to increased perturbation of the fluid flow by the ellipsoid. Applications to DNA sequencing, analysis of single, optically trapped cells and liposomes, and competitive binding, bead-based assays are discussed.

## 2. Experimental details

### 2.1. Apparatus

A schematic diagram of the apparatus is presented in figure 1(a). The sheath flow cuvette (SFC) had a  $250 \times 250$   $\mu\text{m}^2$  square bore channel and one face fabricated to a cover slip thickness ( $\sim 170$   $\mu\text{m}$ ) to accommodate the optical trapping/fluorescence collection objective (MO1). Our sheath flow system is a modification of a design described previously [7]. Briefly, sheath fluid was introduced into the open top of the sheath flow cuvette using a syringe pump. A precision syringe pump (DM-100, ISCO Inc., Lincoln NE, USA) connected to the bottom of the cuvette through a 1.5 m length of 320  $\mu\text{m}$  id fused silica capillary operated in the withdrawal mode provided pulseless flow with precise control over the fluid volumetric flow rate through the flow cell. A short section of fused silica capillary (670  $\mu\text{m}$  outer diameter (od), 540  $\mu\text{m}$  id) positioned at the

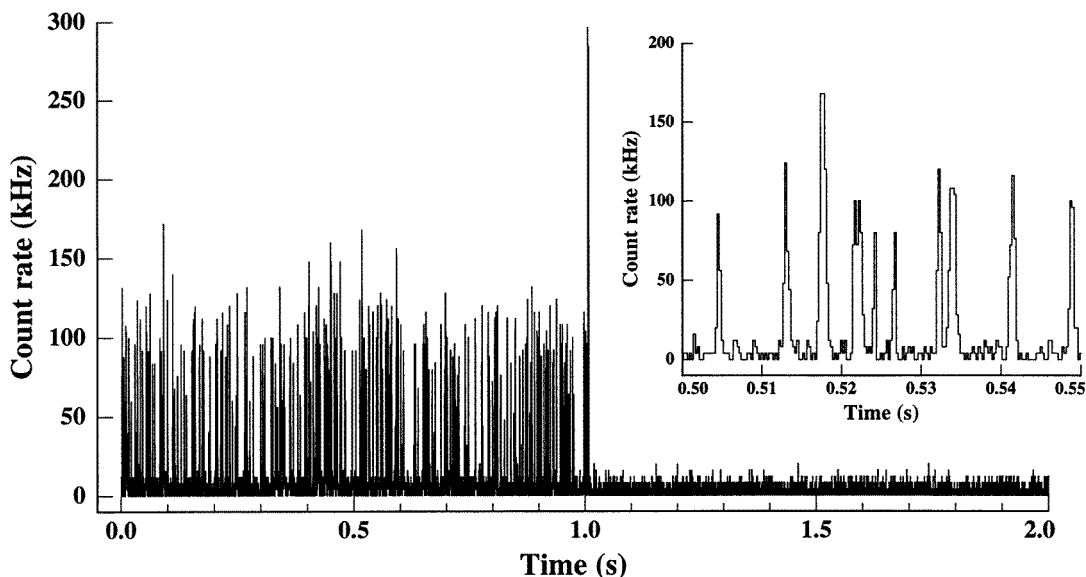


**Figure 2.** Unprocessed data showing photon bursts due to single R6G molecules eluting from a dye stained microsphere optically trapped  $\sim 20 \mu\text{m}$  upstream of a  $10 \mu\text{m}$   $e^{-2}$  diameter detection laser beam. The data are binned into  $250 \mu\text{s}$  time intervals. At  $\sim 1 \text{ s}$  the microsphere is released from the optical trap and falls through the detection laser, as evidenced by the large photon burst. The inset shows an expanded view of the time axis near  $0.5 \text{ s}$ . Experimental conditions: average excitation power,  $7 \text{ mW}$ ; emission bandpass filter,  $550 \pm 15 \text{ nm}$ ; sheath flow velocity through the detection volume,  $\sim 1 \text{ cm s}^{-1}$ ; transit time ( $e^{-2}$ ),  $1 \text{ ms}$ .

top of the flow cell removed excess sheath fluid through an aspirator to regulate the size of the fluid drop at the top of the flow cell. A capillary ( $20 \mu\text{m}$  id,  $90 \mu\text{m}$  od) mounted on a three-axis translation stage, and inserted into the square bore flow channel from the top of the cuvette, was used to introduce microspheres into the sheath flow. The end of the capillary was positioned approximately  $200 \mu\text{m}$  upstream of the detection volume. An actuator allowed the end of the sample introduction capillary to be moved laterally from over the detection volume after a microsphere was trapped.

A water immersion microscope objective (MO1) ( $60\times$ ,  $1.2 \text{ NA}$ , CFN plan apochromat, Nikon Inc., Melville NY, USA) was used for optical trapping and fluorescence collection, similar to the arrangement described by Wang *et al* [18]. This objective was chosen for its ability to form well corrected images of water immersed objects up to  $220 \mu\text{m}$  below a cover slip [19]. A continuous-wave  $\text{Nd}^{+}:\text{YAG}$  laser (4116E, Quantronix Corporation, Smithtown NY, USA) operated at  $1.06 \mu\text{m}$  was used for optical trapping (TL). Approximately  $1 \text{ W}$  of infrared laser light was coupled into a single-mode fiber (SMF) through a  $20\times$  objective (MO5). About half of this light exited the output end of the fiber and  $10\times$  focusing objective (MO2) that were both mounted on a three-axis translation stage to allow precise positioning of the optical trap inside the flow cell. A dichroic beam splitter (DBS), a  $1.06 \mu\text{m}$  dielectric high reflector with  $\sim 70\%$  transmission in the mid-visible, reflected the trapping laser into MO1. Trapping laser powers (power incident on the back of MO1) of approximately  $500 \text{ mW}$  were used for the work presented here.

The excitation source (EL) was a mode-locked  $\text{Ar}^{+}$  laser (2080, Spectra-Physics, Mountain View CA, USA) operated at  $514.5 \text{ nm}$  (pulse width  $< 200 \text{ ps}$ , pulse repetition rate  $82 \text{ MHz}$ ). A spherical lens (L) was used to focus the probe laser at the center of the flow channel. Fluorescence and scattered light collected by MO1 were transmitted through the dichroic beam splitter and imaged onto a  $600 \mu\text{m}$  wide slit (S) to limit the length of the focused probe laser viewed by the detector to  $\sim 10 \mu\text{m}$ . Light transmitted through a bandpass filter (BPF) was focused with a  $32\times$ ,  $0.6 \text{ NA}$  long working distance objective (MO3) onto the active area of a photon-counting avalanche photodiode (APD) (SPCM-200-PQ, EG&G Optoelectronics, Canada). A  $550 \pm 15 \text{ nm}$  bandpass filter with an optical density (OD) of 4 at  $1.06 \mu\text{m}$  was used to pass R6G fluorescence emission. A  $575 \pm 13 \text{ nm}$  bandpass filter was used in combination with a piece of  $2 \text{ mm}$  thick KG-3 glass (OD 3 at  $1.06 \mu\text{m}$ ) to pass fluorescence emission from tetramethylrhodamine isothiocyanate (TRITC) and R6G. The detected photons were processed using time-correlated single photon counting electronics [20, 21] to discriminate against background due to Raman and Rayleigh scattered excitation laser light.

A  $3.5\times$  objective (MO4) was used to image the flow channel onto a CCD video camera (CCDVC). The camera was protected by suitable blocking filters (BF) to attenuate the probe laser and scattered infrared trapping laser light. A  $633 \text{ nm}$  HeNe laser coupled into the optical fiber along with the trapping laser was used to illuminate trapped microspheres.

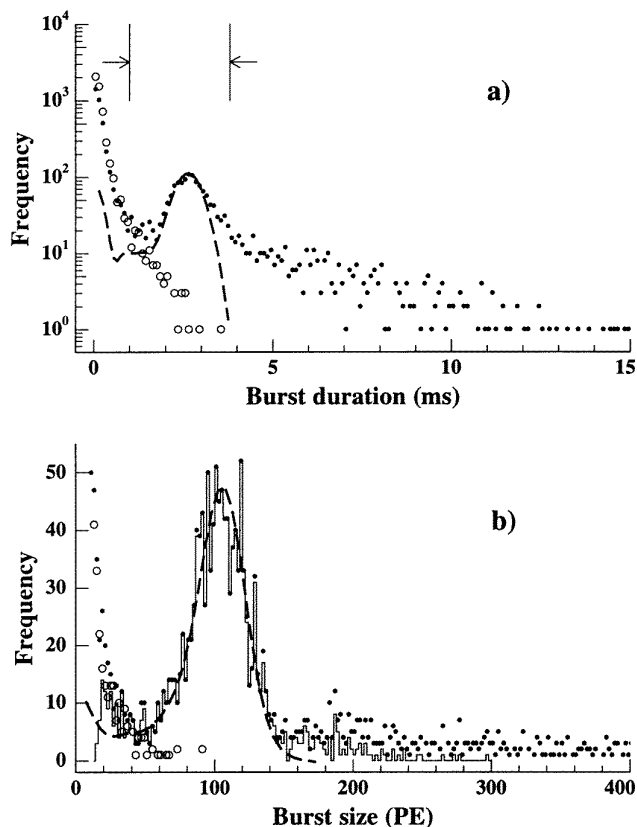


**Figure 3.** (a) A semi-log plot of burst duration distributions (BDDs) compiled from photon burst data collected with a R6G stained microsphere upstream of the detection laser beam (●) and from data collected after the release of the microsphere (○). Both distributions were compiled from 55 s of data. Vertical lines and arrows denote the range of burst durations (1.0–3.8 ms) due primarily to single molecule R6G fluorescence bursts; the majority of shorter bursts are from background, longer bursts are accidental coincidences (more than one R6G molecule in the probe volume simultaneously). The dashed curve shows the BBD generated by the simulation for single R6G molecules without accidental coincidences. (b) Burst size distributions (BSDs) compiled from the same data used for (a). BSD compiled from data recorded with a R6G stained microsphere upstream of the detection volume (●). The peak at 100 PE is due to single R6G molecule fluorescence bursts; bursts greater than 140 PE are accidental coincidences. BSD compiled from data without the microsphere (○). The BSD shown with the full line is compiled from the subset of bursts with durations between 1.0 and 3.8 ms to discriminate against background and accidental coincidences. The dashed curve is the BSD generated by simulation of single R6G fluorescence bursts without accidental coincidences. Experimental conditions: excitation laser beam  $e^{-2}$  diameter, 16  $\mu\text{m}$ ; average power, 10 mW; emission bandpass filter,  $550 \pm 15$  nm; sheath flow velocity through the detection volume,  $\sim 0.5$   $\text{cm s}^{-1}$ ; transit time ( $e^{-2}$ ), 3 ms.

## 2.2. Materials

The sheath fluid was ultra-pure water from a water purification system (Milli-Q plus, Millipore Inc., Bedford MA, USA). Samples consisted of streptavidin coated

polystyrene microspheres (1  $\mu\text{m}$  diameter, Interfacial Dynamics Corporation, Portland, OR, USA) that were stained with R6G or TRITC by suspension in  $1 \times 10^{-4}$  M aqueous dye solutions for several days. The stained microspheres were separated from the concentrated dye solution by centrifugation and resuspended in  $1 \times$  Dulbecco's phosphate-buffered saline solution. For the TRITC/R6G experiment, R6G was added to the TRITC stained microsphere suspension immediately before loading it on the sample introduction capillary. The concentration of R6G was adjusted to give similar elution rates of TRITC and R6G off the microspheres. For the data shown in figure 4, the final R6G concentration in the microsphere suspension was approximately  $1 \times 10^{-7}$  M.

## 2.3. Data analysis

Each detected photon arriving with a delay greater than 1 ns with respect to the excitation laser pulse (gated photon) is recorded. The record consists of arrival times (with respect to the previous gated photon) for each gated photon. A photon burst is evidenced by a series of successive gated photons recorded at a high rate ( $\sim 100$  kHz) compared to the background counting rate ( $\sim 4$  kHz). The algorithm used to search data sets for photon bursts is described in detail elsewhere [20, 21]. For the work presented here, a burst search threshold time of 0.1 ms was used, that is, successive gated photons (photoelectrons) recorded at time intervals of less than 0.1 ms would be considered as a photon burst. Each detected photon burst is characterized by two parameters: (1) the number of photoelectrons comprising the burst (burst size) and (2) the duration of the burst. To reduce contributions due to background bursts and accidental coincidences (a fluorescence burst recorded with two or more analyte molecules in the detection volume simultaneously), bursts were time-filtered, that is, those with durations significantly shorter or longer than the mean molecular transit time across the detection volume were discarded.

A Monte Carlo simulation was used to validate experimental results and to estimate SMD efficiencies [21, 22]. The simulation accounts for spatial variations in the intensity of the excitation laser and optical collection efficiency, photobleaching, optical saturation, and diffusion of analyte molecules in the excitation volume as well as the detection electronics dead time. In the simulation, analyte molecules were introduced into the sheath flow uniformly across a 1  $\mu\text{m}$  diameter in a plane orthogonal to and intersecting the flow axis 20  $\mu\text{m}$  upstream of the center of the excitation volume. Synthetic data generated by the simulation were subjected to the same burst search algorithm (see previously) used to analyze the experimental data. Table 1 lists the parameters used for the simulation.

**Table 1.** Simulation parameters for R6G single molecule detection.

Absorption cross section at 514.5 nm [23]	$2.2 \times 10^{-16} \text{ cm}^2$
Fluorescence quantum yield [24]	0.9
Photodestruction quantum yield [23]	$1.9 \times 10^{-5}$
Saturation intensity	$5.5 \times 10^4 \text{ W cm}^{-2}$
Diffusion constant [12]	$3 \times 10^{-6} \text{ cm}^2 \text{ s}^{-1}$
Average excitation laser power	$10 \times 10^{-3} \text{ W}$
Excitation laser beam diameter ( $e^{-2}$ )	$16 \times 10^{-4} \text{ cm}$
Sample flow velocity	$0.53 \text{ cm s}^{-1}$
Transit time ( $e^{-2}$ )	$(16 \times 10^{-4})/0.53 = 3 \times 10^{-3} \text{ s}$
550 $\pm$ 15 nm bandpass filter transmission	0.27
Detection electronics dead time	$4 \times 10^{-6} \text{ s}$
Photon collection/detection efficiency (excluding bandpass filter transmission factor)	0.06
Average background photon detection rate	$3.6 \times 10^3 \text{ s}^{-1}$

### 3. Results and discussion

#### 3.1. Single molecule detection experiments

Experiments were conducted as follows. The optical trap was aligned to be  $\sim 20 \mu\text{m}$  upstream of the focused excitation laser beam (see figure 1(b)). With the excitation laser blocked, microspheres were injected into the sheath stream. The position of the sample injection capillary was adjusted to cause microspheres to pass through the trapping laser. With the capillary properly positioned the trapping laser captured microspheres in the sample stream ‘on the fly’. Immediately after a microsphere was trapped, the sample stream was shut off, the sample capillary moved laterally from above the probe volume, and the excitation laser unblocked. The capillary was moved to minimize background caused by free dye (not bound to a microsphere) diffusing from the capillary into the sheath flow. Microspheres heavily doped with R6G would initially give large, continuous fluorescence signals. After some seconds, the dye elution rate off the trapped microsphere would fall to a level where single molecule bursts were visible in the data stream and after a few minutes the burst rate approached the background level.

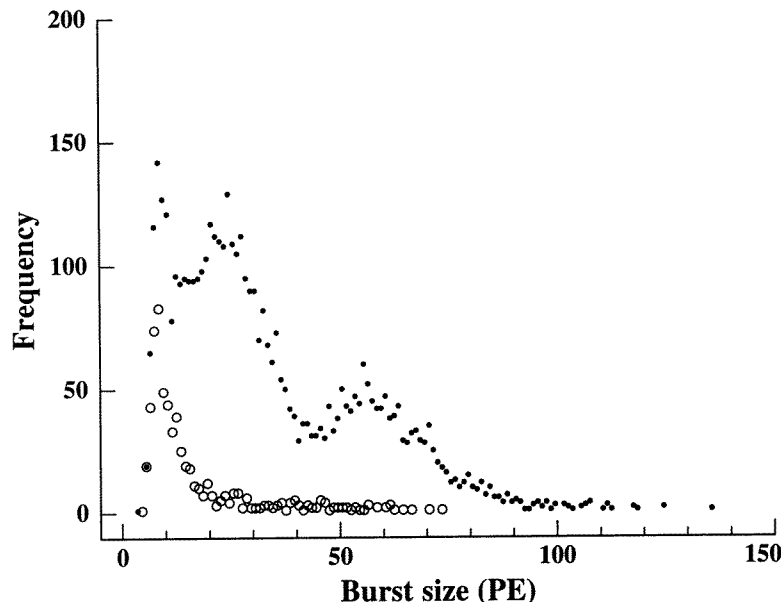
Figure 2 shows unprocessed photon burst data from a R6G stained microsphere held  $\sim 20 \mu\text{m}$  upstream of a  $\sim 1 \text{ pl}$  probe volume. Fluorescence from single R6G molecules crossing the detection volume is visible as photon bursts recorded at peak counting rates of  $\sim 100 \text{ kHz}$ . At  $\sim 1 \text{ s}$ , the trapped microsphere was released and flowed through the probe laser as evidenced by a large photon burst that saturated the detection electronics. The low background, due to residual scattered laser light and fluorescence impurities in the sheath fluid, is evident from the data following the release of the microsphere.

Figure 3(a) shows burst duration distributions (BDDs) compiled from photon burst data collected with and without a R6G stained microsphere upstream of the detection volume. Fluorescence bursts from single R6G molecules

eluting from the microsphere and crossing the detection volume gave a peak in the BDD centered at  $\sim 2.5 \text{ ms}$ . Burst durations in the range 1.0–3.8 ms are due mainly to single R6G molecules. Shorter bursts are due to background and longer bursts arise from accidental R6G molecule coincidences (i.e., more than one R6G molecule in the probe volume simultaneously). The dashed curve shows the BDD expected for single R6G molecules under these conditions; the distribution was compiled from synthetic data generated by the Monte Carlo simulation. In the simulation, single R6G molecules were introduced into the excitation volume at fixed (10 ms) intervals to eliminate accidental coincidences.

Burst size distributions (BSDs) compiled from the same photon burst data are shown in figure 3(b). The peak in BSD compiled from data recorded with a trapped microsphere is again due to fluorescence bursts from R6G molecules eluting from the microsphere and crossing the detection volume individually. Photon bursts larger than 140 PE are primarily due to accidental R6G molecule coincidences inside the detection volume. The dashed curve shows the BSD expected for single R6G molecules without accidental coincidences. A time-filtered BSD compiled from bursts having durations in the range 1.0–3.8 ms is shown with the full line. In general, coincidences have longer burst durations and are suppressed by time filtering. For a burst size threshold of 45 PE, we estimate from the simulation that 92% of the R6G molecules eluting from the microsphere are detected. With the time filter the detection efficiency drops to 91%. According to the simulation, 16% of the R6G molecules photobleach prior to crossing the excitation volume and, of these, approximately half are detected. The background burst rate (measured with the trap empty) for this burst size threshold is  $\sim 0.5 \text{ s}^{-1}$ .

In other work we have demonstrated efficient detection and identification at the single molecule level of two fluorescent dyes (R6G and TRITC) having similar photophysical properties [22]. The two fluorophores can



**Figure 4.** Time-filtered BSD compiled from single TRITC and R6G molecules eluting off of a  $1\ \mu\text{m}$  diameter microsphere. BSD compiled from 42 s of data collected with the dye stained microsphere upstream of the probe laser (●). The peak at  $\sim 26$  PE is due to fluorescence bursts from single TRITC molecules, the peak at  $\sim 55$  PE is from single R6G bursts. BSD compiled from 42 s of data taken following the release of the microsphere (○). The distributions were compiled from bursts with durations between 0.4 and 1.8 ms (mean burst duration, 1.4 ms) to discriminate against background and accidental coincidences. Experimental conditions: excitation laser beam  $e^{-2}$  diameter,  $16\ \mu\text{m}$ ; average power, 20 mW; emission filters,  $575 \pm 13$  nm bandpass and 2 mm thick KG-3 glass filter; sheath flow velocity through the detection volume,  $\sim 1\ \text{cm s}^{-1}$ ; transit time ( $e^{-2}$ ), 3 ms.

be distinguished by differences in their single molecule fluorescence burst sizes and intra burst fluorescence decay rates measured using a single excitation wavelength and single detection channel. In order for this method to work, the sample stream must be sufficiently narrow and well aligned with respect to the detection volume to resolve the single molecule fluorescence burst size distributions of the two species. Here we demonstrate detection and discrimination of single TRITC and R6G molecules eluting from a trapped microsphere. Figure 4 shows the time-filtered BSD from an experiment conducted with a microsphere stained with R6G and TRITC held upstream of the detection volume. The peak at  $\sim 26$  PE is due to fluorescence bursts from single TRITC molecules, the peak at  $\sim 55$  PE is due to single R6G molecule fluorescence bursts. Even though the BPF was chosen to match the emission maximum of TRITC, measured R6G single molecule fluorescence bursts are larger than TRITC bursts. This is due to R6G's larger ( $\sim 1.4\times$ ) absorption cross section at 514.5 nm and higher fluorescence quantum yield (0.9 versus 0.35 for TRITC [25]).

### 3.2. Flow calculations

To illustrate and compare the effects of the microsphere and capillary tip on the sample stream diameter downstream of the introduction point, we undertook detailed calculations of the sample stream evolution for a diffusing species under flow conditions similar to those of our experiments.

The spatial ( $r$ ) and time ( $t$ ) dependent concentration distribution  $c(r, t)$  of dye in the liquid obeys the following partial differential equation:

$$\frac{\partial c}{\partial t} + \mathbf{u} \cdot \nabla c = D \Delta c \quad (1)$$

where  $\mathbf{u}$  is the space (but not time) dependent velocity of the liquid flow, and  $D$  is the diffusion constant of the dye in solution. Since we are interested in a stationary concentration profile, the time derivative on the left-hand side is set to zero. One then has to solve the resulting time-independent equation with appropriate boundary conditions. First, one has to find the velocity profile  $\mathbf{u}$ , which is a solution of the stationary Navier–Stokes equations. Because we are interested in flows with very low Reynolds numbers, only solutions of the linearized Navier–Stokes equations are considered (Stokes flow). In the modeling, the flow profiles of two well known solutions of the linearized Navier–Stokes equations were used: the flow around a sphere, and the flow around a prolate ellipsoid of revolution [26]. The geometrical parameters of the ellipsoid were determined by fitting it to the shape of a typical pulled capillary tip (see figure 3 in [4]) used for sample introduction. For a sufficiently small inner radius of the capillary, the ellipsoid should give a good approximation of the real flow profile. Since the walls of the flow cell are far away ( $\sim 100\ \mu\text{m}$ ) from the injection capillary and the region of interest ( $\sim 10\ \mu\text{m}$ ), a uniform flow velocity  $u_\infty$

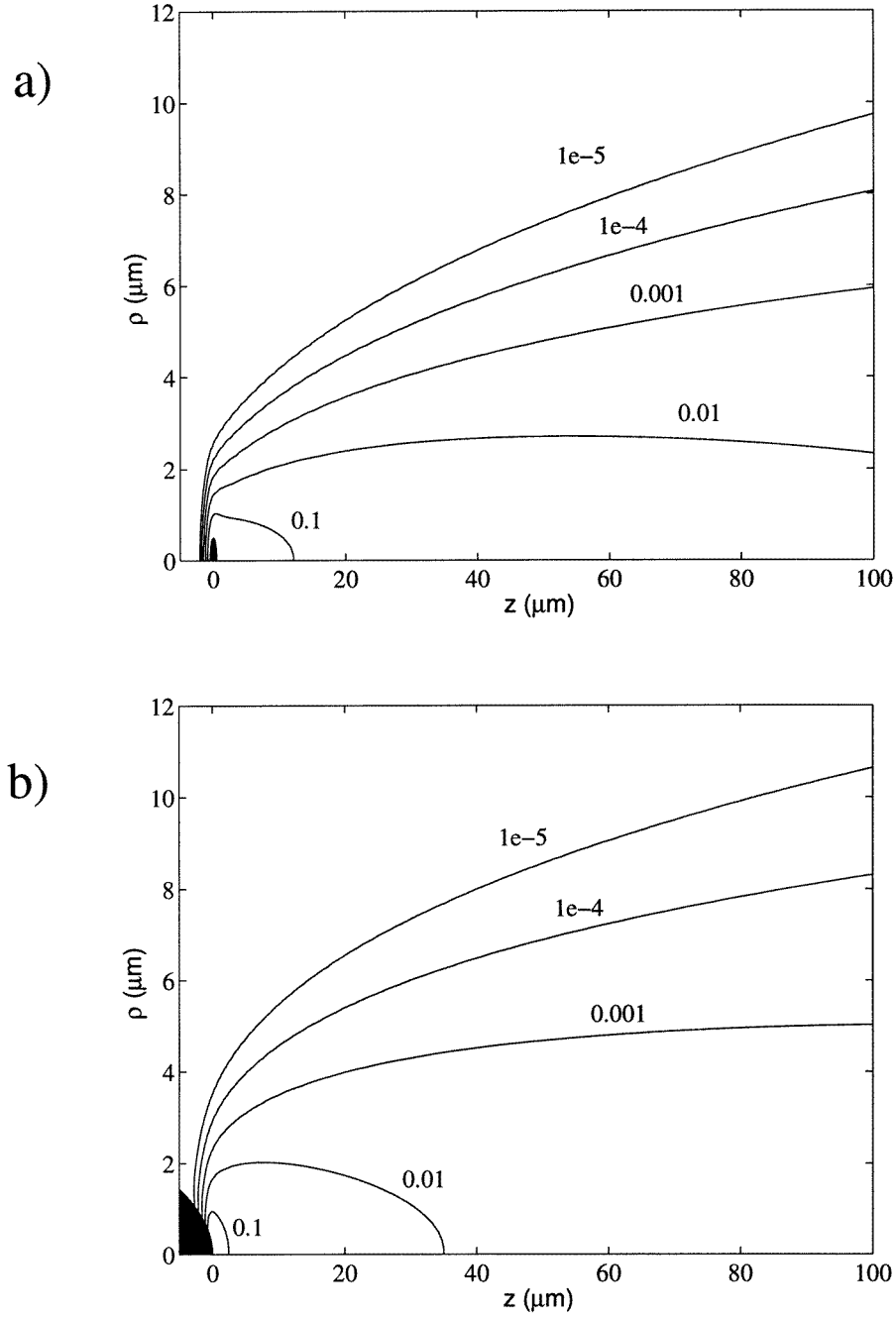


**Figure 5.** (a) A contour plot of the stationary concentration profile for a sphere (radius  $0.5 \mu\text{m}$ ) with unit surface concentration in a uniform flow with  $u_\infty = 1 \text{ cm s}^{-1}$  and  $D = 3 \times 10^{-6} \text{ cm}^2 \text{ s}^{-1}$ . Contours are shown for relative concentrations of 0.1, 0.01, 0.001,  $1 \times 10^{-4}$  and  $1 \times 10^{-5}$ . (b) A contour plot of the stationary concentration profile for an ellipsoid of revolution (long half-axis  $810 \mu\text{m}$ , short half-axis  $13 \mu\text{m}$ ) with unit surface concentration within a region of  $\rho \leq 0.5 \mu\text{m}$  in a uniform flow with  $u_\infty = 1 \text{ cm s}^{-1}$  and  $D = 3 \times 10^{-6} \text{ cm}^2 \text{ s}^{-1}$ .

along the symmetry axis of the flow cell at infinite distance from the sphere (ellipsoid) was assumed. The flow profile for a sphere of radius,  $R$ , in cylindrical coordinates  $(\rho, \phi, z)$  reads

$$u_\rho = \frac{3u_\infty R}{4s} \left[ \left( \frac{R}{s} \right)^2 - 1 \right] \sin \theta \cos \theta$$

$$u_z = u_\infty - \frac{u_\infty R}{4s} \left[ \left( \frac{R}{s} \right)^2 (1 - 3 \cos^2 \theta) + 3(1 + \cos^2 \theta) \right]$$

$$u_\phi = 0 \quad (2)$$

where the abbreviations  $s = \sqrt{\rho^2 + z^2}$  and  $\theta = \arctan(\rho/z)$  were used.

In the case of a prolate ellipsoid of revolution with long

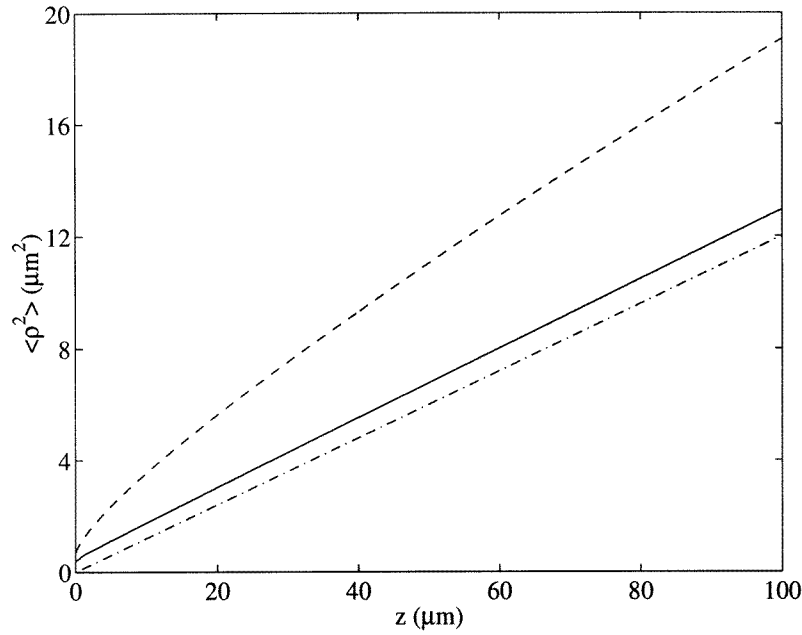


**Figure 6.** Development of the square of the effective sample stream radius,  $\rho_{eff}^2(z)$ , for sample streams from the sphere (—) and the ellipsoid of revolution (- - -) in a uniform flow. For comparison, the result for a point source is shown (- · -).

half-axis,  $c$ , and short half-axis,  $a$ , the profile has a more complicated structure:

$$\begin{aligned} u_\rho &= \frac{\Gamma \sin 2\theta}{2\Sigma^2 \sinh \xi} [\mu^2 \cosh 2\xi - c^2 - a^2] \\ u_z &= v_\infty + \frac{\Gamma}{\Sigma^2} \left[ (\mu^2 \cos 2\theta - c^2 - a^2) \cosh \xi \right. \\ &\quad \left. - 2 \left( 1 + \frac{c^2}{\mu^2} \right) \Sigma^2 \ln \left( \frac{\sinh \xi}{\cosh \xi + 1} \right) \right] \\ u_\phi &= 0 \end{aligned} \quad (3)$$

where the following abbreviations were used:

$$\begin{aligned} \mu &= \sqrt{c^2 - a^2} \\ \Sigma &= \mu \sqrt{\sinh^2 \xi + \sin^2 \theta} \\ \Gamma &= \frac{u_\infty}{2} \left[ \frac{c}{\mu} + \left( 1 + \frac{c^2}{\mu^2} \right) \ln \left( \frac{a}{c + \mu} \right) \right]^{-1} \end{aligned} \quad (4)$$

and the connection between  $\xi, \theta$  and the cylindrical coordinates is implicitly given by

$$\rho = \mu \sinh \xi \sin \theta \quad z = \mu \cosh \xi \cos \theta. \quad (5)$$

For both of the above velocity profiles, the diffusion-convection equations (1) were solved numerically. In the case of the sphere, a constant dye concentration (equal to one) at the surface was assumed, and in the case of the ellipsoid, a constant dye concentration (equal to one) on the downstream tip of the ellipsoid in a region  $\rho \leq R$  was assumed.

The numerical solution of (1) for a sphere with radius  $R = 0.5 \mu\text{m}$  is shown in figure 5(a). The corresponding

result for an ellipsoid of revolution with  $c = 810 \mu\text{m}$ ,  $a = 13 \mu\text{m}$ , and  $R = 0.5 \mu\text{m}$  is shown in figure 5(b). The flow velocity at infinity was equal to  $u_\infty = 1 \text{ cm s}^{-1}$ , and the diffusion constant was set to  $D = 3 \times 10^{-6} \text{ cm}^2 \text{ s}^{-1}$ .

The square of the effective sample stream radius,  $\rho_{eff}^2$ , at axial position,  $z$ , is defined by

$$\rho_{eff}^2(z) = \langle \rho^2 \rangle = \frac{\int d\rho \rho^3 c(\rho, z)}{\int d\rho \rho c(\rho, z)}. \quad (6)$$

The development of this quantity along the  $z$ -axis for both the flow around the sphere and the ellipsoid are shown in figure 6. Note that the sample stream diameter ( $2\rho_{eff}$ ) from the sphere is always smaller than that from the ellipsoid. This is a consequence of the increased perturbation of the flow field by the ellipsoid compared to the sphere. The flow pattern downstream of the ellipsoid requires more distance (time) to re-establish a uniform flow pattern ( $u_\infty$ ) than it does for the sphere. Dye eluting from the end of the ellipsoid spends more time accelerating to  $u_\infty$  and has more time to diffuse radially. To demonstrate the minimal perturbation of the flow field by the microsphere, we have plotted  $\rho_{eff}^2(z)$  for a species diffusing from a *point* source located at  $(z, \rho) = (0, 0)$ :

$$\rho_{eff}^2(z) = \frac{4Dz}{u_\infty}. \quad (7)$$

The major difference between the two is an offset due to the finite extent of the microsphere. From figure 6, the ratio of sample stream diameters at  $z = 20 \mu\text{m}$  downstream of the ellipsoid and microsphere is  $4.7/3.4 = 1.3$ . The sample stream diameter  $20 \mu\text{m}$  downstream of the microsphere is only  $\sim 10\%$  larger than that from a point source.

#### 4. Conclusions

We have demonstrated efficient single molecule detection of fluorescent species eluting from a 1  $\mu\text{m}$  diameter microsphere optically trapped upstream of a focused excitation laser beam. Because of the small size of the trapped microsphere, the point of sample introduction can be positioned very close to the detection volume, to minimize diffusional broadening of the sample stream, without degradation of the detection SBR due to scattered laser light and fluorescence from the microsphere. These factors and the minimal perturbation of the sheath fluid flow pattern by the microsphere allow smaller sample stream diameters in the detection volume than are attainable using capillary sample introduction. Smaller sample stream diameters result in higher SMD efficiencies as well as improved resolution of single molecule fluorescence burst sizes useful for species identification at the single molecule level.

We are currently using optical traps in our single molecule DNA sequencing effort [27,28]. Previously, we used micro-pipettes to hold DNA-laden microspheres upstream of the detection volume for experiments demonstrating exonuclease cleavage of fluorescently-labeled DNA in flow [8,29]. Replacement of the micro-pipette with an optical trap has greatly simplified sample loading. Preliminary experiments show a significant reduction in the fluorescence burst background rate. A large component of the background was due to fluorescent impurities adsorbed to the surface of the micro-pipette. These experiments also show improved SMD efficiencies due to smaller stream diameters than were attained in earlier work using micro-pipettes.

In general, the method is useful for monitoring the release of minute quantities of a fluorescent species initially bound to a solid substrate. An example would be a flow-based competitive binding assay [30]. Here, antibodies for a specific antigen bound to a solid support are saturated with a fluorescent analog of the antigen. A buffer containing the antigen is flowed past the support and the fluorescent antigen analog is detected downstream of the support. Detection of the analog indicates its displacement from the antibody by the antigen. For a weakly bound antigen and correspondingly small displacements, it would be advantageous to measure fluorescence from the displaced fluorescent analog instead of a small reduction in fluorescence of the remaining fluorescent analog bound to the support. Additionally, SMD of the fluorescent analog would greatly reduce the amount of antigen and antibody required for such assays. One can also visualize SMD assays of fluorescently-labelled species released from optically trapped cells or liposomes.

#### Acknowledgments

This work was supported by the Los Alamos Center for Human Genome Studies under United States Department

of Energy contract W-7405-ENG-36. NPM gratefully acknowledges the US Department of Energy for permitting and coordinating his assignment at Los Alamos National Laboratory through its Technical Leadership Development Program. JE greatly acknowledges the support of the German Academic Exchange Service granting him his stay at Los Alamos National Laboratory. We gratefully acknowledge Michael Bern's group at the University of California, Irvine, for technical discussions and assistance with regard to optical trapping.

#### References

- [1] Shera E B, Seitzinger N K, Davis L M, Keller R A and Soper S A 1990 Detection of single fluorescent molecules *Chem. Phys. Lett.* **174** 553–7
- [2] Barnes M D, Whitten W B and Ramsey J M 1995 Detecting single molecules in liquids *Anal. Chem.* **67** A418–23
- [3] Keller R A, Ambrose W P, Goodwin P M, Jett J H, Martin J C and Wu M 1996 Single-molecule fluorescence analysis in solution *Appl. Spectrosc.* **50** A12–32
- [4] Goodwin P M, Ambrose W P and Keller R A 1996 Single-molecule detection in liquids by laser-induced fluorescence *Accounts Chem. Res.* **29** 607–13
- [5] Harris T D and Lytle F E 1983 Analytical applications of laser absorption and emission spectroscopy *Ultrasensitive Laser Spectroscopy* ed D S Kliger (New York: Academic) ch 7, pp 369–433
- [6] Zarrin F and Dovichi N J 1985 Sub-picoliter detection with the sheath flow cuvette *Anal. Chem.* **57** 2690–2
- [7] Li L Q and Davis L M 1995 Rapid and efficient detection of single chromophore molecules in aqueous solution *Appl. Opt.* **34** 3208–17
- [8] Goodwin P M *et al* 1995 Progress towards DNA sequencing at the single molecule level *Exp. Tech. Phys.* **41** 279–94
- [9] Soper S A, Mattingly Q L and Vegunta P 1993 Photon burst detection of single near-infrared fluorescent molecules *Anal. Chem.* **65** 740–7
- [10] Lee Y H, Maus R G, Smith B W and Winefordner J D 1994 Laser-induced fluorescence detection of a single-molecule in a capillary *Anal. Chem.* **66** 4142–9
- [11] Guenard R D, King L A, Smith B W and Winefordner J D 1997 Two channel sequential single-molecule measurement *Anal. Chem.* **69** 2426–33
- [12] Rigler R, Widengren J and Mets Ü 1993 Interactions and kinetics of single molecules as observed by fluorescence correlation spectroscopy *Fluorescence Spectroscopy: New Methods and Applications* ed O S Wolfbeis (Berlin: Springer) ch 2, pp 13–24
- [13] Mets Ü and Rigler R 1994 Submillisecond detection of single rhodamine molecules in water *J. Fluoresc.* **4** 259–64
- [14] Nie S M, Chiu D T and Zare R N 1994 Probing individual molecules with confocal fluorescence microscopy *Science* **266** 1018–21
- [15] Nie S M, Chiu D T and Zare R N 1995 Real-time detection of single-molecules in solution by confocal fluorescence microscopy *Anal. Chem.* **67** 2849–57
- [16] Zander C and Drexhage K H 1997 Sequential counting of single molecules in a microcapillary *Proc. Soc. Photo-opt. Ins.* **2980** 545–50

- [17] Demas J N, Wu M, Goodwin P M, Affleck R L and Keller R A 1997 Fluorescence detection in hydrodynamically focused sample streams: reduction of diffusional defocusing by association of analyte with high molecular weight species *Appl. Spectrosc.* in press
- [18] Wang W, Liu Y, Sonek G J, Berns M W and Keller R A 1995 Optical trapping and fluorescence detection in laminar flow streams *Appl. Phys. Lett.* **67** 1057–9
- [19] Brenner M 1994 Imaging dynamic events in living tissue using water immersion objectives *Am. Laborat.* **26** 14–19
- [20] Goodwin P M, Affleck R L, Ambrose W P, Jett J H, Johnson M E, Martin J C, Petty J T, Schecker J A, Wu M and Keller R A 1996 Detection of single fluorescent molecules in flowing sample streams *Computer Assisted Analytical Spectroscopy* ed S D Brown (Chichester: Wiley) ch 3, pp 61–80
- [21] Goodwin P M, Wilkerson C W Jr, Ambrose W P and Keller R A 1993 Ultrasensitive detection of single molecules in flowing sample streams by laser-induced fluorescence *Proc. Soc. Photo-opt. Ins.* **1895** 79–89
- [22] Van Orden A, Machara N P, Goodwin P M and Keller R A 1997 Single molecule identification in flowing sample streams by fluorescence burst size and intra-burst fluorescence decay rate *Anal. Chem.* in press
- [23] Soper S A, Nutter H L, Keller R A, Davis L M and Shera E B 1993 The photophysical constants of several fluorescent dyes pertaining to ultrasensitive fluorescence spectroscopy *Photochem. Photobiol.* **57** 972–7
- [24] Georges J, Arnaud N and Parise L 1996 Limitations arising from optical saturation in fluorescence and thermal lens spectrometries using pulsed laser excitation: application to the determination of the fluorescence quantum yield of Rhodamine 6G *Appl. Spectrosc.* **50** 1505–11
- [25] Whitaker J E, Haugland R P, Ryan D, Hewitt P C, Haugland R P and Prendergast F G 1992 Fluorescent rhodol derivatives: versatile, photostable labels and tracers *Anal. Biochem.* **207** 267–79
- [26] Lamb H 1945 *Hydrodynamics* (New York: Dover)
- [27] Ambrose W P *et al* 1993 Application of single molecule detection to DNA sequencing and sizing *Ber. Bunsen. Phys. Chem.* **97** 1535–42
- [28] Goodwin P M, Cai H, Jett J H, Ishaug-Riley S L, Machara N P, Semin D J, Van Orden A and Keller R A 1997 Application of single molecule detection to DNA sequencing *Nucleosides Nucleotides* **16** 543–50
- [29] Schecker J A, Goodwin P M, Affleck R L, Wu M, Martin J C, Jett J H, Keller R A and Harding J D 1995 Flow-based continuous DNA sequencing via single molecule detection of enzymatically cleaved fluorescent nucleotides *Proc. Soc. Photo-opt. Ins.* **2386** 4–12
- [30] Kusterbeck A W, Wemhoff G A, Charles P T, Yeager D A, Bredehorst R, Vogel C W and Ligler F S 1990 A continuous-flow immunoassay for rapid and sensitive detection of small molecules *J. Immunol. Med.* **135** 191–7